Asian Journal of Chemistry; Vol. 37, No. 4 (2025), 873-881

ASIAN JOURNAL OF CHEMISTRY

https://doi.org/10.14233/ajchem.2025.33254

Tunable Blue-Yellow Emission in $LaInO_3$:Bi^{3+},Dy^{3+} Phosphors *via* Polyol Synthesis for Advanced LED Applications

A. Ganesh[1,*], K. Suresh[1], K. Sujatha[2] and B.V. Naveen Kumar[3]

[1]Department of Humanities & Basic Sciences, G. Pulla Reddy Engineering College (Autonomous), Kurnool-518007, India
[2]Department of Physics, V.V. Giri Government Degree Kalasala, Dumpagadapa (Affiliated to Adikavi Nannaya University), Akividu-534235, India
[3]Department of Physics, University of the Free State, Bloemfontein 9300, South Africa

*Corresponding author: E-mail: ambaliganesh85@gmail.com

Received: 23 December 2024; *Accepted*: 10 March 2025; *Published online*: 29 March 2025; AJC-21949

The polyol synthesis method was employed to prepare $LaInO_3$ perovskite phosphors doped with Bi^{3+} (x = 1, 3, 5 at.%) and co-doped with Dy^{3+} (y = 1-5 at.%). The X-ray diffraction (XRD) confirmed the formation of a pure orthorhombic $LaInO_3$ phase in annealed samples. Morphological analysis revealed spherical agglomerates with some irregularities, ranging in size from 60 to 90 nm. The reduction of energy band gap on doping ions into lattice using DFT studies. The energy-dispersive spectroscopy (EDS) confirmed the successful incorporation of Bi^{3+} and Dy^{3+} ions into the $LaInO_3$ lattice. The photoluminescence (PL) studies demonstrated that Bi^{3+}-doped $LaInO_3$ exhibited a broad blue emission peak at 432 nm due to the $^3P_1 \rightarrow {}^1S_0$ transition of Bi^{3+} ions. On the other hand, $LaInO_3$ doped with Dy^{3+} exhibited distinctive emissions at 482 nm (blue) and 584 nm (yellow), which correspond to the $^4F_{9/2} \rightarrow {}^6H_{15/2}$ and $^4F_{9/2} \rightarrow {}^6H_{13/2}$ transitions of Dy^{3+} ions, respectively. The optimized sample composition is found to be $LaInO_3$: 3 at.% Bi^{3+}, 3 at.% Dy^{3+} demonstrated enhanced emission intensities due to energy transfer from Bi^{3+} to Dy^{3+} ions making it a promising candidate for advanced LED applications.

Keywords: Oxide, Perovskite, Photoluminescence, WLED, Energy transfer.

INTRODUCTION

A significant volume of investigation has focused on the development of single-phase white luminescent materials, due to their crucial functions in white light emitting diodes (WLEDs) and display technologies [1-5]. In this context, the oxide-based materials have demonstrated remarkable luminescent properties, a significant threshold for optical damage, as well as exceptional chemical and thermal stability [6-10]. The unique structural features and fascinating luminous capabilities of the narrow bandgap (2.2 eV) semiconducting compound $LaInO_3$ have attracted a lot of attention, especially for uses in solid-state lighting [11]. Many researchers have made their investigations by doping with rare earth dopants as activator ions, which are fascinating since they glow brightly in the visible and near-infrared ranges [12-15].

White light emitting diodes (WLEDs) can be produced by utilizing Dy^{3+} activator ions, which are abundant in the yellow and blue regions. Nevertheless, phosphors activated by Dy^{3+} ions exhibit very low light efficiency due to their emissions. The transfer of energy from sensitizers to activators enhances the luminescence efficiency and intensity of the activator ion. The luminous effectiveness of Dy^{3+} ions within inorganic host materials is enhanced by co-doping Bi^{3+} ions, according to numerous research [2-5]. The emission of Bi^{3+} ions exhibits a broad spectral range covering blue and green regions, with the peak intensity in the blue wavelength depending on the host lattice. This behaviour is significantly influenced by environmental factors, including covalence, coordination number and site symmetry, which affect the outer $6s^2$ electronic configurations of Bi^{3+} ions. Significant absorption is observed during the transitions from $^1S_0$ to $^3P_1$ and $^1P_1$, suggesting that activator ion emission intensity could be enhanced through efficient energy transfer [16,17]. Furthermore, the overlap between emission (sensitizer) and excitation (activator) constitutes a significant prerequisite for effective energy transfer.

Based on our interest in the perovskite-based single-phase materials for white light applications, in this study, phosphor

powders of $LaInO_3$ co-doped with Bi^{3+} and Dy^{3+} were synthesized and characterized using the polyol technique. The effects of this co-doping on the powder properties are examined. In regard to its use in white light luminescence, a thorough analysis was carried out into the photoluminescence properties and energy transfer processes of Bi^{3+} and Dy^{3+} co-doped $LaInO_3$ phosphor. The examination of CIE coordinates demonstrates improvements in colour quality which are suitable for UV-based WLED uses.

EXPERIMENTAL

Synthesis: A straightforward wet-chemical process called the polyol approach was employed to synthesize pure $LaInO_3$, Bi-doped and Bi-Dy co-doped nanophosphors. the stoichiometric proportions of lanthanum nitrate, indium nitrate, bismuth nitrate and dysprosium nitrate were mixed in 20 mL of ethylene glycol, which plays a crucial role as both a reducing and capping agent followed by the addition of urea (2 g) and stirred well. The solution temperature must be maintained between 120-140 ºC for 2 h. The solutions were collected by washing, centrifugation and dust-free drying. The dried samples were calcined in a furnace at 1000 ºC and ground with an agate mortar and pestle.

Characterization: The structural and morphological features of the obtained samples were studied using powder X-ray diffraction (XRD) and scanning electron microscopy (SEM). The X-ray diffraction (XRD) studies were carried out using a Philips powder X-ray diffractometer (model PW 1071) with Ni filtered Cu-*K*α radiation in a scanning range of 10º to 90º. A Carl Zeiss sigma VP SEM equipped with a field emission gun operated at 5 kV was used to collect SEM images of the samples. Photoluminescence (PL) emission, excitation and lifetime spectra were measured at room temperature using a 450 W Xe lamp from an Edinburgh Instrument (FLSP 920 system).

RESULTS AND DISCUSSION

Phase formation and microstructure: The XRD results for undoped and $LaInO_3$: 3 at.% Bi^{3+}, 3 at.% Dy^{3+} phosphors are shown in Fig. 1. The XRD results showed that the diffraction patterns are indexed to the pure orthorhombic phase (JCPDS No. 08-0148) of $LaInO_3$ that falls under *Pnma* space group (#62) [18,19], with no signs of additional or impurity phases present. Table-1 shows the results of using POWDERX software to determine the lattice characteristics of the produced nanophosphors. Using Scherrer's equation, the crystallite diameters of all the samples were determined and found to be between 70 and 90 nm. Fig. 2a shows the SEM image of the optimized sample composition *i.e.*, $LaInO_3$: 3 at.% Bi^{3+} and 3 at.% Dy^{3+} phosphor and reveal that the particles, ranging in size from 60 to 90 nm, exhibit a non-uniform spherical shape. The calcination process may have caused the phosphor particles to aggregate. The energy dispersive X-ray spectroscopy (EDS) analysis provided a clear picture of the sample composition and proved to be in excellent agreement with the sample composition (Fig. 2b).

Computational studies: The Vienna *ab initio* Simulation, a method based on plane waves, was used to conduct periodic density functional theory (DFT) simulations of $LaInO_3$ in order

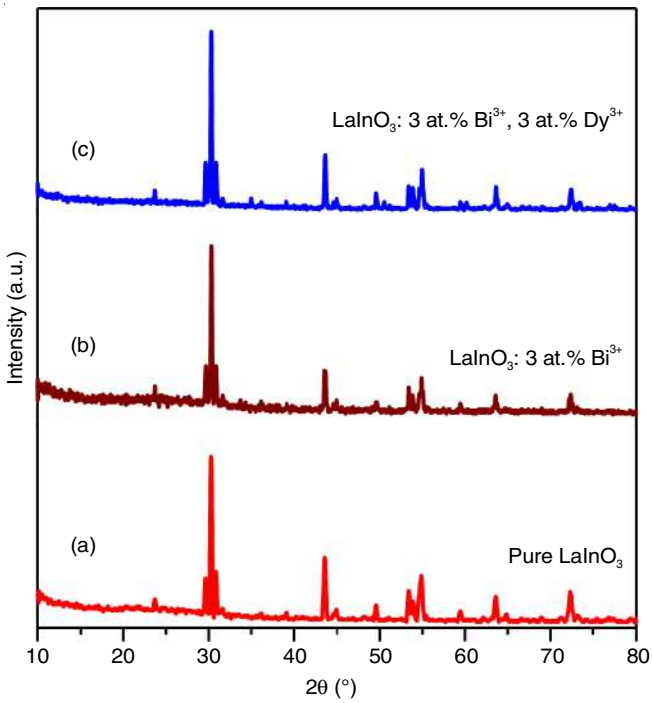

Fig. 1. XRD patterns corresponding to (a) $LaInO_3$, (b) $LaInO_3$: 3 at.% Bi^{3+} and (c) $LaInO_3$: 3 at.% Bi^{3+}, 3 at.% Dy^{3+} nanophosphors

TABLE-1
UNIT CELL PARAMETERS OF UNDOPED $LaInO_3$, $LaInO_3$: 3 at.% Bi^{3+} AND $LaInO_3$: 3 at.% Bi^{3+}, 3 at.% Dy^{3+}

Composition	a (Å)	b (Å)	c (Å)	V^3 $(Å)^3$
$LaInO_3$	5.782	8.336	5. 999	289.14
$LaInO_3$: 3 at.% Bi^{3+}	5.775	8.245	5.928	282.26
$LaInO_3$: 3 at.% Bi^{3+}, 3 at.% Dy^{3+}	5.770	8.015	5.815	268.92

to investigate the impact of Bi and Dy doping on its electronic structure. Using the generalized gradient approximation (GGA) of Perdew–Burke\Ernzerhof (PBE), the exchange-correlation energy density functional was processed [20]. For determining the band structure of pure $LaInO_3$, a more precise method than the PBE functional band gaps was employed. The GGA+U was used to describe 'La' strongly linked 5d electrons with a U_{eff} value of 6.0 eV [21].

To optimize the $LaInO_3$ unit cell structure with 20 orthorhombic (*Pnma*) atoms, a force cut-off of 0.005 eV/Å was utilized. Consistent with previous results [22], the optimized unit cell structure is displayed in Fig. 3a with parameters a = 5.774 Å, b = 6.006 Å and c = 8.347 Å. In the optimized unit cell structure, InO_6 units have In-O distances of 2.19 Å (a-b) and 2.22 Å (along c), with In-O-In angels of 143.065º (a-b) and 140.225º (c). The minimum and maximum Ln-O distance in LaO_8 units are 2.380 Å and 3.012 Å. In Fig. 3b, the electronic band structure of $LaInO_3$ calculated using PBE functional yielded a band gap of 2.71 eV, which is consistent with previous results using the same functional but significantly underestimated compared to the experimental band gap of 4.8 eV. The electronic band structure and density of states (DOS) of pure system were estimated using the HSE06 functional and shown in Fig. 3c-d. The measured band gap from HSE06 functional

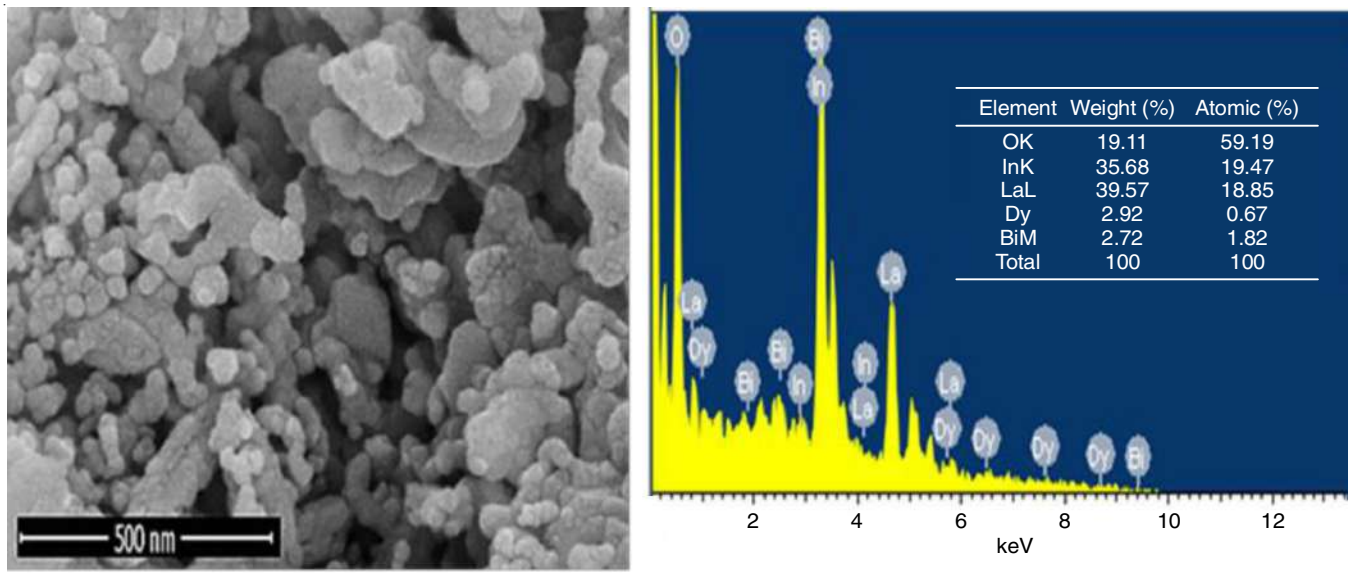

Element	Weight (%)	Atomic (%)
OK	19.11	59.19
InK	35.68	19.47
LaL	39.57	18.85
Dy	2.92	0.67
BiM	2.72	1.82
Total	100	100

Fig. 2. SEM image and EDS spectra of Bi^{3+} and Dy^{3+} co-doped $LaInO_3$ nanophosphors

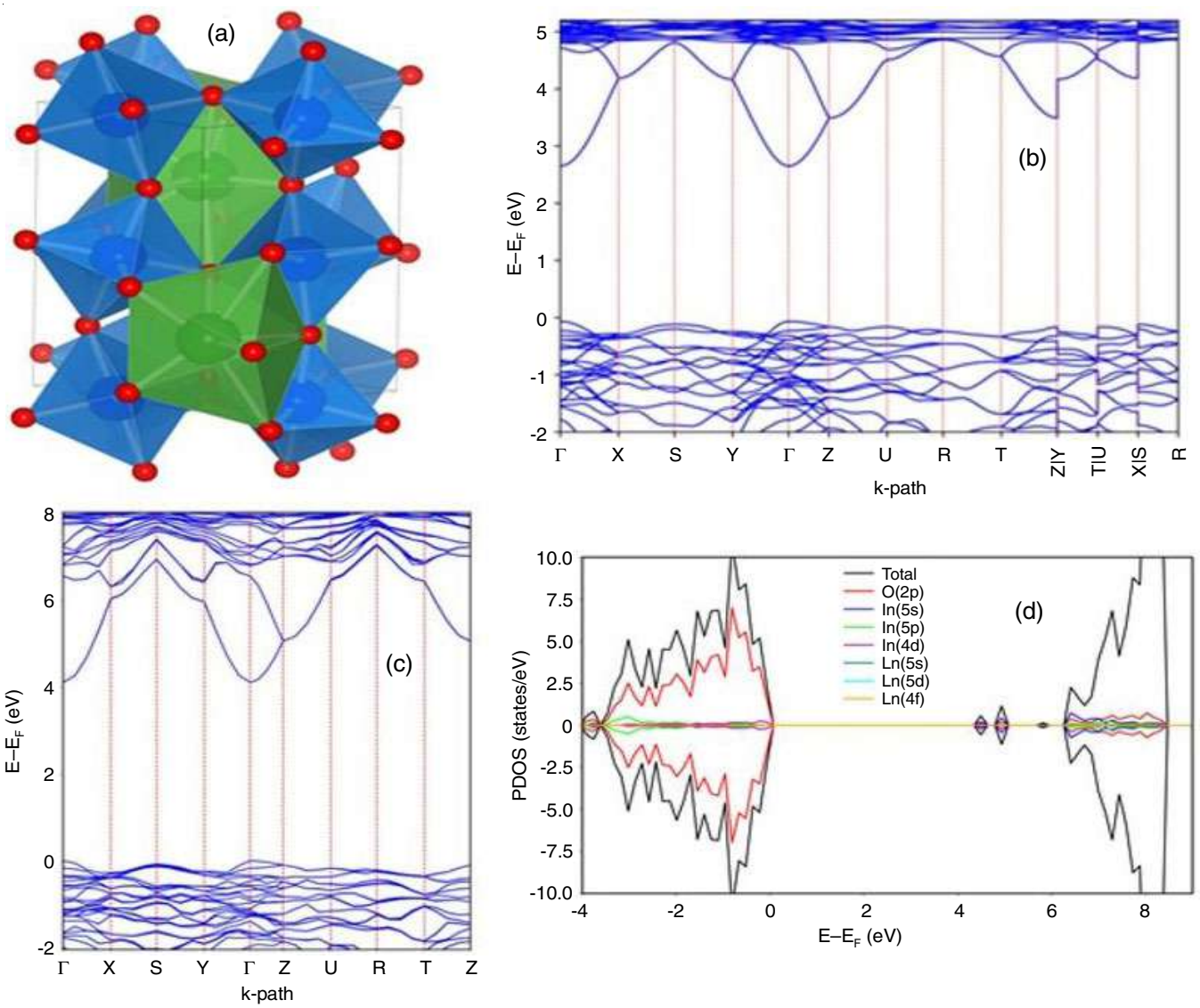

Fig. 3. (a) Optimized unit cell structure (InO_6: blue, LaO_8: green), (b) electronic band structure from PBE and (c) electronic band structure and density of stated from HSE06 of $LaInO_3$

was 4.49 eV, which matches the experimental results. The projected density of states (PDOS) shows that O 2p states dominate the valence band, with In 4*d* and 5*p* states contributing little. The bottom of the conduction band is largely In 5*s* and O 2*p* states. The effect of Bi, Dy and Bi- , Dy co-doping was studied using a 160-atom 2 × 2 × 2 super cell. Fig. 4 shows the optimal structures for Bi and Dy substitutional doping at Dy site, which was energetically favourable. Bi-doped $LaInO_3$ has a band gap of 2.599 eV, down from 2.715 eV in pure $LaInO_3$. Doping with Dy did not significantly lower the band gap (2.710 eV from 2.715 eV in pure).

Fig. 5 shows the total and projected density of state (DOS) on Bi states in Bi-doped $LaInO_3$ to explain the band gap reduction. The PDOS of Bi shows that Bi 6*s*, 5*p* and 5*d* states contribute to the top of the valence band. The structure with relative energies for co-doping Bi and Dy in three relative positions were optimized as shown in Fig. 5. Structure with Bi and Dy at longer distances is energetically minimal compared to structure with them at nearer La sites. The electronic band structure of Bi and Dy co-doped system is essentially identical to Bi-doped system with band gap of 2.584 eV (Fig. 5).

Photoluminescence properties of bismuth single doped $LaInO_3$ phosphors: Fig. 6a-b shows the emission and excitation spectra of Bi-singly doped $LaInO_3$ samples. Monitoring excitation spectra at λ_{em} = 432 nm revealed a large peak maximum at 330 nm. The observed phenomenon was Bi^{3+} ion $^1S_0$ to $^3P_1$ transition. The observed pattern in the emission spectra at 432 nm is a result of the $^3P_1$ - $^1S_0$ transition of Bi^{3+} ions when excited at 330 nm [23]. Fig. 6c shows the decay and steady state graphs that match. As the concentration of Bi^{3+} ions increased, the intensity of emission band at 432 nm peaked at 3.0% Bi^{3+} ions and then decreased as a result of the concentration quenching effect. The two-exponential lifetime estimates for $LaInO_3$:*x* at.% Bi^{3+} samples were 297, 332 and 270 ns, respectively for *x* = 1, 3 and 5 at.%, confirming the results. The steps to determine the decay lifetime values are outlined as follow. When the emission and excitation bands of Bi^{3+} and Dy^{3+} ions overlap, as demonstrated in the as-prepared samples (Fig. 7), an effective energy transfer (ET) occurs. The emission bands of Bi^{3+} encompass the excitation bands of Dy^{3+}, resulting in the observed phenomena.

Photoluminescence properties of Bi^{3+}, Dy^{3+} co-doped $LaInO_3$ phosphors: Fig. 8a shows $LaInO_3$ emission spectra doped with 3 at.% Bi^{3+} and changing Dy^{3+} concentrations (*y* = 1, 2, 3, 5). Similar excitation spectra are shown in Fig. 8b. The emission spectra for $LaInO_3$: 3 at.% Bi^{3+}, (*y* = 1, 2, 3, 5 at.%), Dy^{3+} show blue to yellow lines due to the presence of Bi^{3+} and Dy^{3+} ions at λ_{ex} = 330 nm. The intensity of Bi^{3+} emission signi-

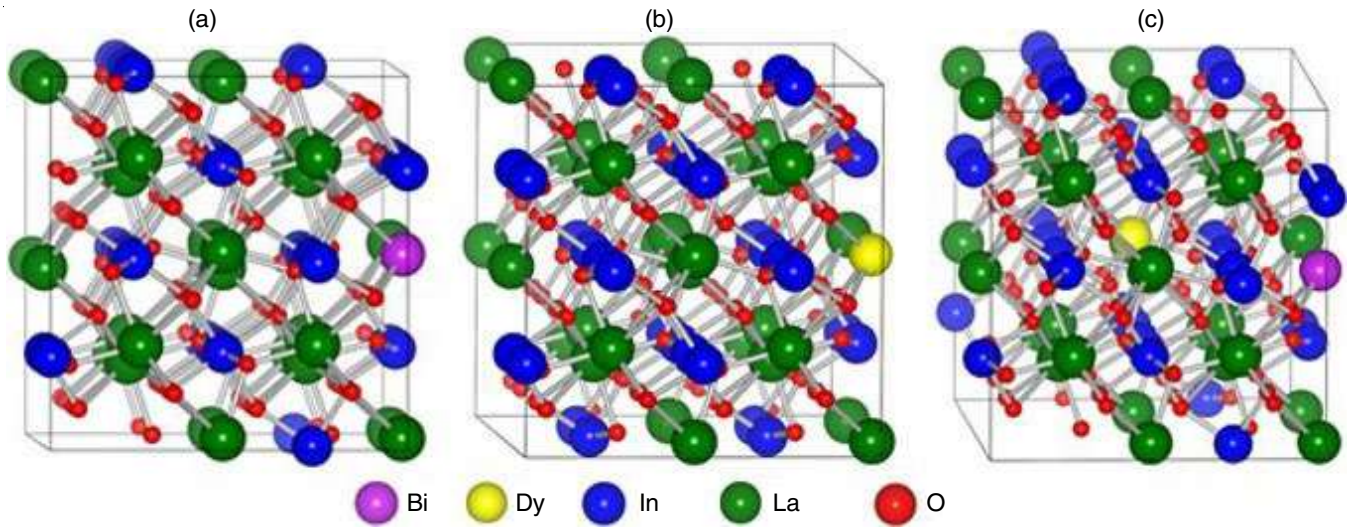

Fig. 4. Optimized minimum energy structure of (a) Bi doped, (b) Dy doped and (c) Bi & Dy co-doped $LaInO_3$ 2 × 2 × 2 super cells

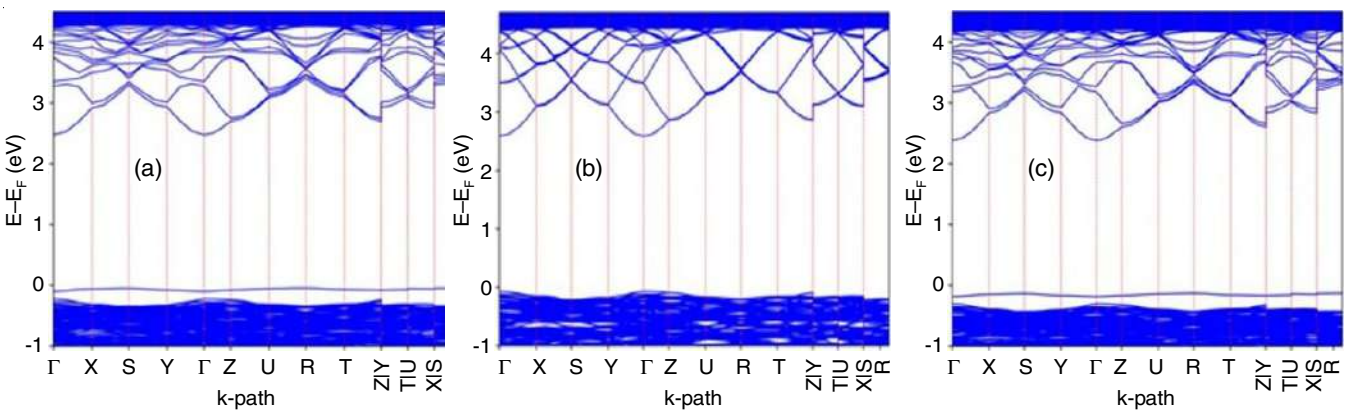

Fig. 5. Electronic band structure of (a) Bi doped, (b) Dy doped and (c) Bi & Dy co-doped $LaInO_3$ calculated using PBE functional

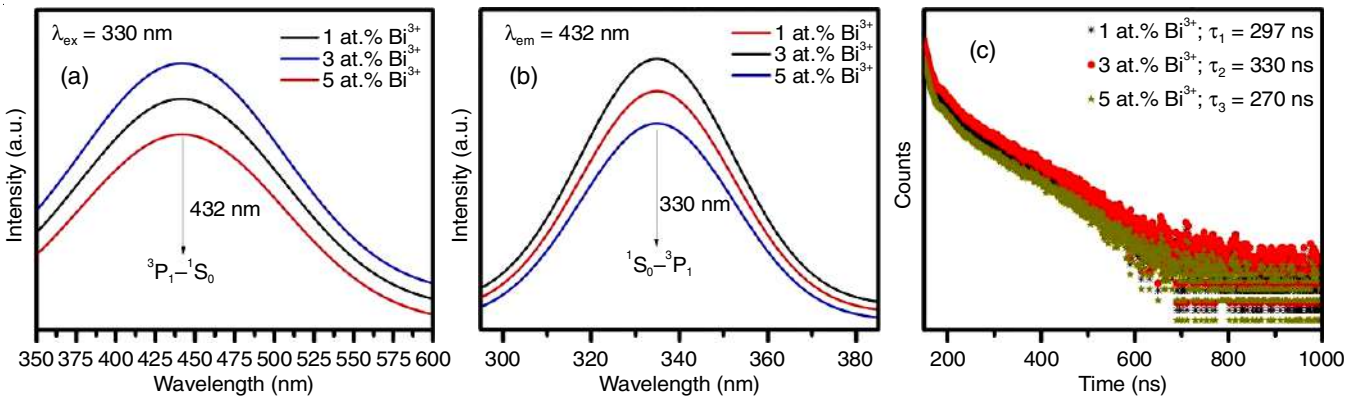

Fig. 6. Photoluminescence (a) emission, (b) excitation and (c) decay curves of $LaInO_3$:Bi^{3+} (1, 3, 5 at.%) samples

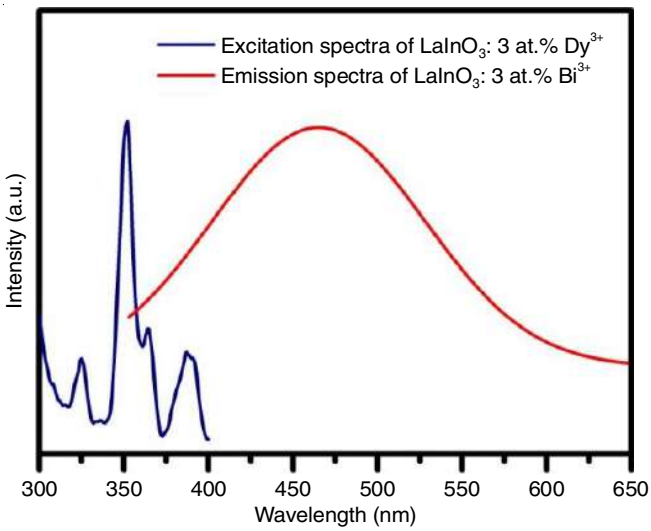

Fig. 7. Spectral overlap of excitation spectrum (λ_{em} monitored at 576 nm) of $LaInO_3$: Dy^{3+} (3 at.%) and emission spectrum of $LaInO_3$: Bi^{3+} (3 at.%) (λ_{ex} with 330 nm) samples

ficantly diminishes when the concentration of Dy^{3+} is altered, while maintaining Bi^{3+} at 3%. On the other hand, as the concentration of Dy^{3+} increases, the emission intensity peaks at 3% Dy^{3+} and subsequently drops. The energy transitions and cross relaxation of Dy^{3+} ions are responsible for this concentration quenching action. The photoluminescence intensity of these kind of material decreases during cross relaxation due to the exchange contact, radiation re-absorption or interactions between several multipoles [24]. The distinctive $^4F_{9/2}$–$^6H_{13/2}$ emission levels of Dy^{3+} are shown in the excitation spectra at λ_{em} = 584 nm. Moreover, a broad band centered around 330-335 nm is attributed to Bi^{3+} ions. Importantly, the co-doping of Bi^{3+} affects the Dy^{3+} ion, which causes a small shoulder absorption band to peak at 335 nm (Fig. 6b). This shows that the excited Bi^{3+} ions efficiently transmit energy (ET) to the Dy^{3+} ions, sensitizing the Dy^{3+} ions. Fig. 9a clearly shows the changes in Bi^{3+} emission intensity as a function of Dy^{3+} concentrations. Similalry, Fig. 9b shows the comparitive emission spectra between single doped $LaInO_3$: Dy^{3+} and $LaInO_3$: Bi^{3+}/Dy^{3+} ions in order to determine the effect of Bi^{3+} doping on the enhancement of PL intensity. As a result, the $LaInO_3$ phosphor compound photoluminescence emission was enhanced.

Lifetime measurements of Bi^{3+}, Dy^{3+} co-doped $LaInO_3$ phosphors: Fig. 10a shows samples of $LaInO_3$ (3 at.% Bi^{3+}, *y*

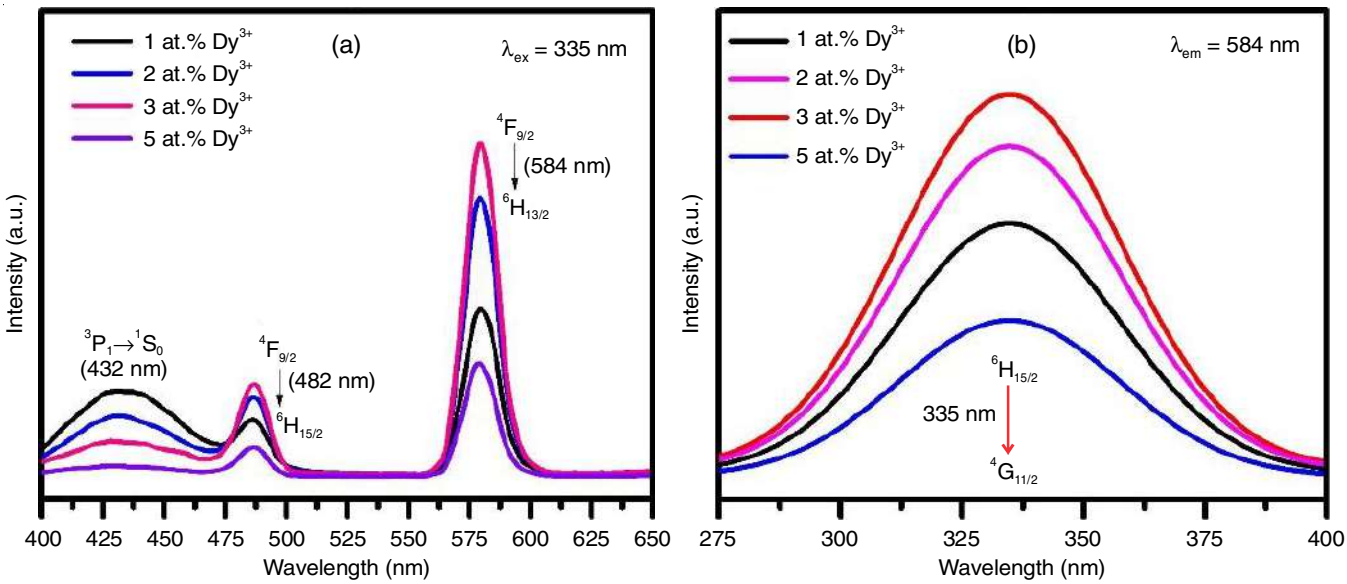

Fig. 8. Photoluminescence (a) emission and (b) excitation spectra of $LaInO_3$: 3 at.% Bi^{3+}; *y* at.% (y = 1, 2, 3, 5 at.%) Dy^{3+} samples

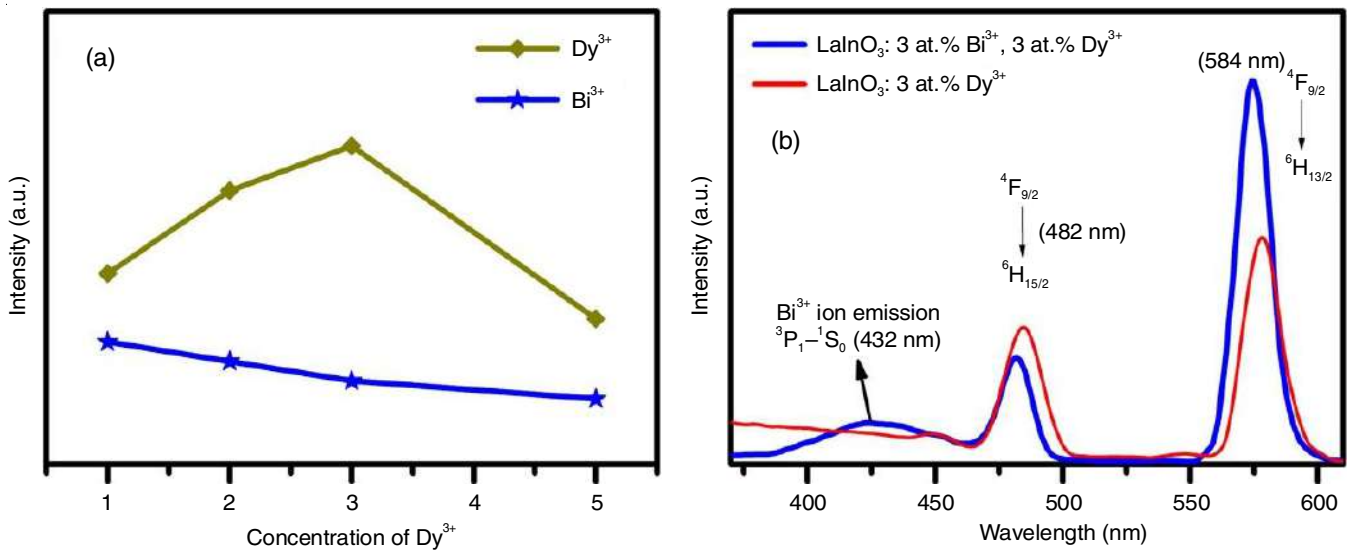

Fig. 9. (a) Intensity variation of Bi^{3+} as a function of Dy^{3+} ions and (b) comparison of single doped Dy^{3+} $LaInO_3$ emission spectra w.r.to Bi^{3+}/Dy^{3+} co-doped $LaInO_3$ emission spectra

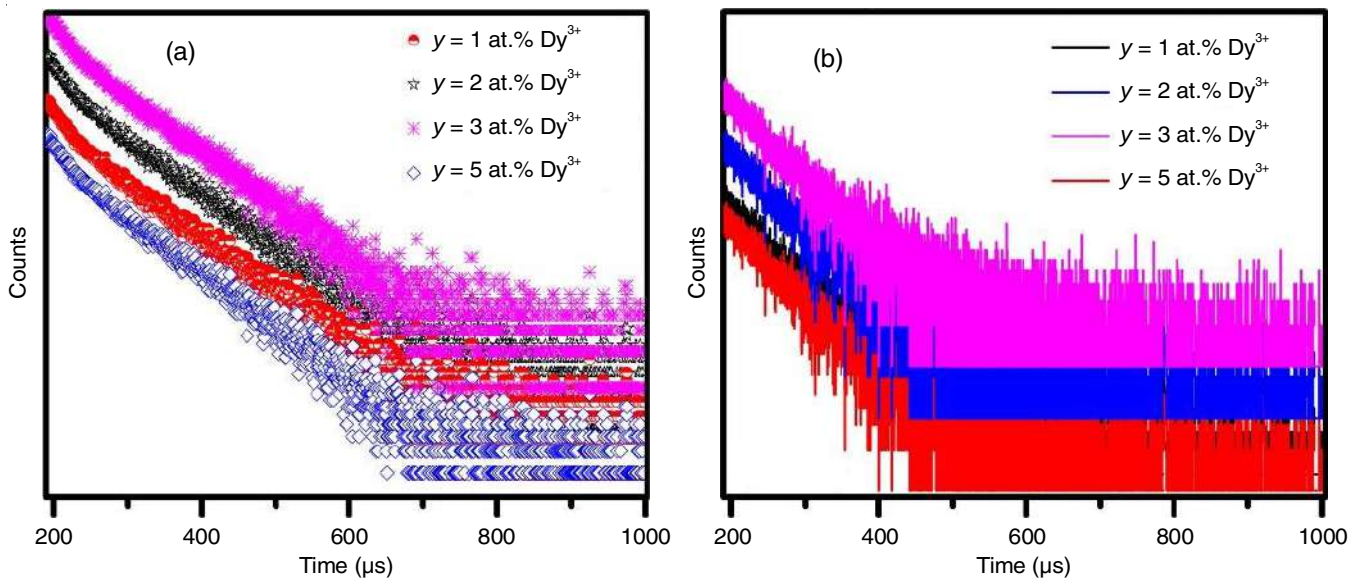

Fig. 10. Lifetime decay graphs of (a) Bi^{3+} and (b) Dy^{3+} in $LaInO_3$: 3 at.% Bi^{3+}, *y* at.% (*y* = 1, 2, 3, 5) Dy^{3+} samples

at.% (*y* = 1, 2, 3, 5) Dy^{3+} were used to study the life time decay dynamics. The following equation was determined to effectively correspond with the bi-exponential luminescence decay curves generated for all samples:

$$I = A_1 \exp\left(\frac{-t}{\tau_1}\right) + A_2 \exp\left(\frac{-t}{\tau_2}\right) \quad (1)$$

In this equation, I represent the luminescence intensity with respect to time (t), while the two decay components of decay time are denoted by τ_1 and τ_2, respectively. The constants A_1 and A_2 are also included in the formulation. The average decay times of the respective samples were estimated based on the specified parameters using the following formula:

$$\tau = \frac{A_1\tau_1^2 + A_2\tau_2^2}{A_1\tau_1 + A_2\tau_2} \quad (2)$$

The calculated luminescence decay times (τ) of Bi^{3+} are approximately 220, 201, 192 and 179 ns for $LaInO_3$: 3 at.% Bi^{3+}; y at.% (*y* = 1, 2, 3, 5) Dy^{3+} samples. The decay times for the corresponding Dy^{3+} are 226, 240, 283 and 239 μs as shown in Fig. 10b. The increase of Dy^{3+} concentration results in an accelerated decline of Bi^{3+} emission, a phenomenon attributed to energy transfer from Bi^{3+} to Dy^{3+}.

Using the following equation the energy transfer (ET) efficiency (η_{ET}) of Bi^{3+}-Dy^{3+} can be estimated:

$$\eta_{ET} = 1 - \frac{\tau_s}{\tau_{so}} \quad (3)$$

where τ_s and τ_{so} are the lifetime values of sensitizer Bi^{3+} in the presence and absence of activator, respectively. Table-2 details the values of the energy-transfer efficiency η_{ET} from Bi^{3+} to Dy^{3+} for $LaInO_3$. In addition, the energy transfer efficiency as

TABLE-2
ENERGY TRANSFER EFFICIENCY OF THE PREPARED PHOSPHOR POWDER

Prepared phosphor powder	*y*	Lifetime values (μs)	η_{ET} (%)
$LaInO_3$: 3 at.% Bi^{3+}, *y* at.% Dy^{3+}	1	2.20	34
	2	2.01	39
	3	1.92	42
	5	1.79	46

a function of decay values is shown in Fig. 11. Resonant energy transfer in phosphors occurs *via* two distinct types of interactions: exchange and multi-polar interaction, which move electrons from a sensitizer (Bi^{3+}) to an activator (Dy^{3+}). It is essential to keep the critical distance between the sensitizer and activator below 5 Å in order for energy transfer to occur through the exchange contact. An electric multi-polar interaction is anticipated to occur once the transfer distance reaches the critical distance. An approximation of the critical distance R_c between Bi^{3+} and Dy^{3+} in the $LaInO_3$ matrix can be obtained by applying the following equation:

$$R_c \approx 2\left(\frac{3V}{4\pi\chi_c Z}\right)^{1/3} \quad (4)$$

where Z represents the number of activator ions within the unit cell; X_c is the total critical value of dopant ions and V is the volume of unit cell.

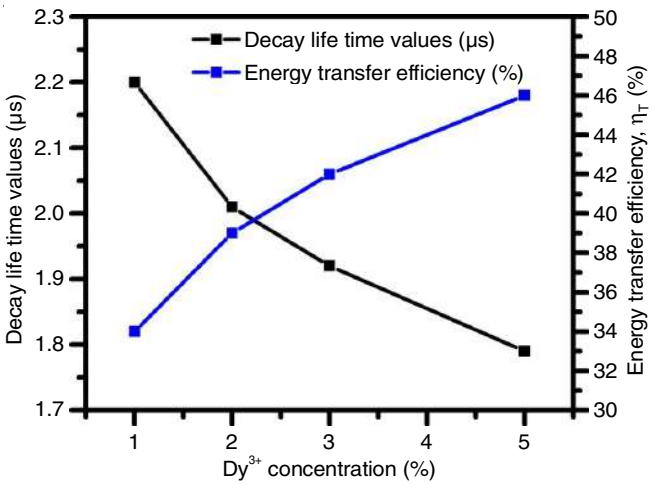

Fig. 11. Decay values *vs.* efficiency w.r.to Dy^{3+} concentration

Utilizing the parameters V = 289.63 $Å^3$ and Z = 2 for the $LaInO_3$ host, along with the optimum dopant ion concentration (X_c = 0.06 for Bi^{3+}-Dy^{3+} system), the 'R_c' between Bi and Dy was estimated as 16.64 Å. It is unlikely that an exchange interaction will result in energy transfer as the measured values are much more than 5 Å. As a result, the energy transfer in $LaInO_3$ from Bi^{3+} to Dy^{3+} is probably heavily influenced by the multi-polar interaction. This relationship can be easily determined by applying Reisfeld's approximation and Dexter's energy-transfer description of multi-polar interaction.

$$\frac{I_{so}}{I_s} \propto C^{\frac{\alpha}{3}} \quad (5)$$

where I_{so} stands for Bi^{3+} lifetime at a given concentration in $LaInO_3$ and I_s for the Bi^{3+} lifetime in the presence of Dy^{3+}. The Dy^{3+} concentration is represented by variable C, while the electric dipole-dipole, electric quadrupole-quadrupole and electric quadrupole-quadrupole interactions are indicated by the values 6, 8 and 10 of the variable α. The optimal linear behaviour for the $I_{so}/I_s \sim C^{\alpha/3}$ (C > 1%), as shown in Fig. 12, was attained at α = 6. This shows that electric dipole-dipole interaction transfers energy from Bi^{3+} to Dy^{3+}. The CIE chromaticity coordinates for pure 3 at.% Bi^{3+} and $LaInO_3$:3 at.% Bi^{3+}, y at.% Dy^{3+} (where *y* = 1, 2, 3, 5) doped $LaInO_3$ phosphors are shown in Fig. 13. Furthermore, Table-3 outlines the photometric variables of the $LaInO_3$ sample, determined using colour calculator software. The CIE diagram illustrates a transition of the CIE colour coordinates from a vibrant blue to a yellowish region, passing through white, as the concentration of Dy^{3+} changes. This observation

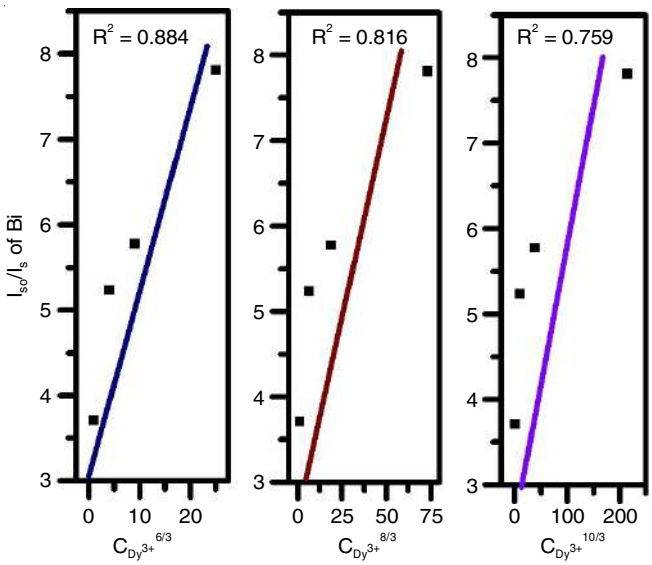

Fig. 12. Dependence of I_{so}/I_s (of Bi^{3+}) on $C^{6/3}$, $C^{8/3}$ and $C^{10/3}$ for Dy^{3+}

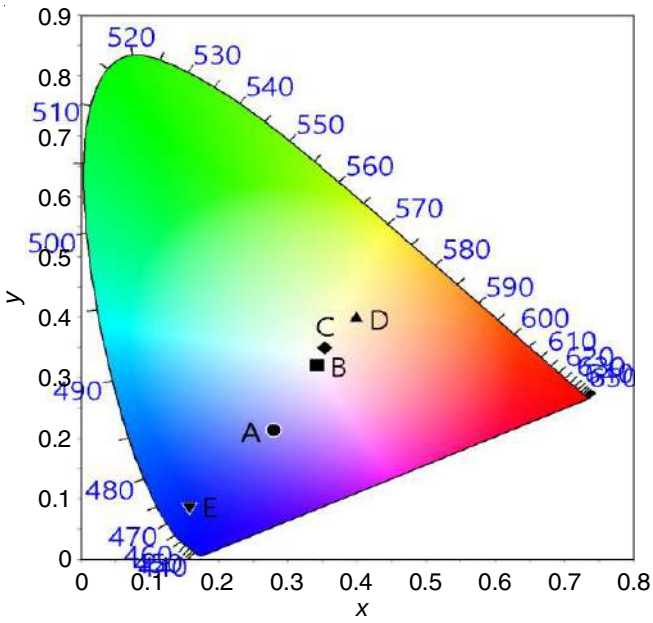

Fig. 13. CIE chromaticity diagram of Bi^{3+} and Dy^{3+} doped $LaInO_3$ phosphors

TABLE-3
PHOTOMETRIC PARAMETERS OF PREPARED PHOSPHOR POWDER

Prepared phosphor powder	y	Symbol	CIE coordinates		Colour
			X	Y	
$LaInO_3$: 3 at.%Bi^{3+}, *y* at.% Dy^{3+}	1	A	0.2792	0.2135	Bluish
	2	B	0.3415	0.3209	White
	3	C	0.3533	0.3498	White
	5	D	0.3982	0.3992	Yellowish
$LaInO_3$: *x* at.% Bi^{3+}	*x* = 3	E	0.1564	0.0891	Deep Blue

suggests that the synthesized phosphor holds promise as a single phase phosphor for use in WLEDs and field display fields under UV excitation.

Energy transfer (ET) mechanism: Fig. 14 depicts the energy transfer system that has been suggested. The electrons of Bi^{3+} ions undergo a transition from $^1S_0$ to $^3P_1$ in response to stimulation from ultraviolet light. Afterwards, these excited electrons are lowered to the ground state by non-radiative processes. The energy is transferred from the $^3P_1$ level of Bi^{3+} to the $^4G_{11/2}$ level of Dy^{3+} through cross-relaxation. The intensity of Dy^{3+} emissions may be enhanced by co-doping with Bi^{3+} ions. The blue light emitted by some Bi^{3+} ion electrons that return to the ground state can absorb energy from $^6H_{15/2}$ of Dy^{3+} ground state levels. Higher energy levels are excited and energy is transferred throughout this process as a result of the observed spectra overlapping. The accelerated electrons, through non-radiative processes, attain the $^4G_{11/2}$ level of Dy^{3+} before returning to the ground state, resulting in the emission of yellowish spectral lines.

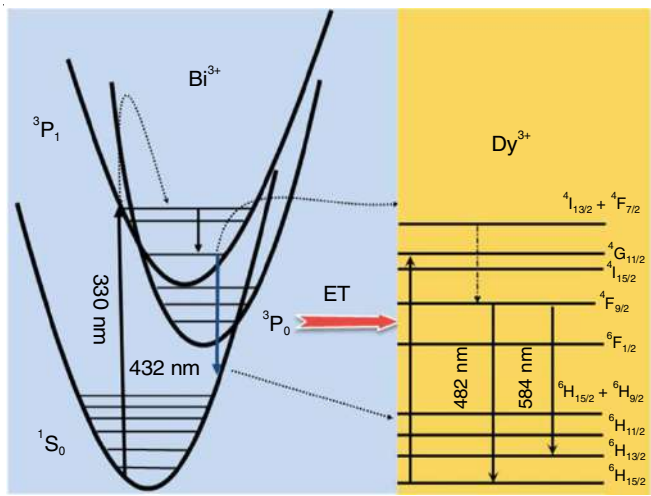

Fig. 14. Energy level diagram of $LaInO_3$:Bi^{3+}:Dy^{3+} nanophosphors

Conclusion

The polyol technique was used to produce Bi^{3+} and Dy^{3+}-doped $LaInO_3$. The luminescence and energy transfer processes of Bi^{3+} and Dy^{3+} were studied. The X-ray diffraction shows that annealed samples have entirely crystallized into $LaInO_3$ orthorhombic. Morphological analysis shows that the particles are spherical agglomerates between 60 and 90 nm in size and shape. The EDS examination showed that Bi^{3+} and Dy^{3+} ions were incorporated into $LaInO_3$ host material. Periodic density functional theory (DFT) simulations utilizing plane wave-based Vienna *ab initio* simulation program (VASP) were conducted to elucidate the influence of Bi^{3+} and Dy^{3+} ions on the electronic structure of $LaInO_3$. The electronics of the co-doped system with Bi^{3+} and Dy^{3+} have a band gap of 2.584 eV, similar to that of the Bi^{3+}-doped system. The $^3P_1$–$^1S_0$ transition of Bi^{3+} ions causes the blue emission peak at 432 nm in Bi^{3+}-doped $LaInO_3$. The transitions from $^4F_{9/2}$ - $^6H_{15/2}$ and $^6H_{13/2}$ of Dy^{3+} ions cause blue and bright yellow emissions at 482 and 584 nm, respectively. The optimal sample was $LaInO_3$: 3 at.% Bi^{3+}; 3 at.% Dy^{3+}. The considerable enhancement in Dy^{3+} emission achieved by Bi^{3+} co-doping allows LED and display technologies to use Dy^{3+} doped phosphors. Thus, electric dipole-dipole interactions transfer resonance energy from Bi^{3+} to Dy^{3+}. The CIE chromatic colour characteristics show that the colour of the sample goes from deep blue to yellowish to white, suggesting that the generated phosphor could be a WLED single-phase phosphor.

CONFLICT OF INTEREST

The authors declare that there is no conflict of interests regarding the publication of this article.

REFERENCES

1. M.K. Tsang, G. Bai and J. Hao, *Chem. Soc. Rev.*, **44**, 1585 (2015); https://doi.org/10.1039/C4CS00171K
2. L. Tian, J. Shen, T. Xu, L. Wang, L. Zhang, J. Zhang and Q. Zhang, *RSC Adv.*, **6**, 32381 (2016); https://doi.org/10.1039/C6RA04761K
3. S.F. Lai, Z.W. Yang, J.Y. Liao, J.B. Qiu, Z.G. Song, Y. Yang and D.C. Zhou, *Mater. Res. Bull.*, **60**, 714 (2014); https://doi.org/10.1016/j.materresbull.2014.09.049
4. W. Zhang, S.X. Liu, Z.F. Hu, Y.L. Liang, Z.Y. Feng and X. Sheng, *Mater. Sci. Eng. B*, **187**, 108 (2014); https://doi.org/10.1016/j.mseb.2014.05.006
5. L. Tian, L. Wang, L. Zhang, Q. Zhang, W. Ding and M. Yu, *J. Mater. Sci.: Mater. Electron.*, **26**, 8507 (2015); https://doi.org/10.1007/s10854-015-3522-1
6. T. Samuel, C.S. Kamal, K. Sujatha, V. Veeraiah, Y. Ramakrishana and K.R. Rao, *Optik*, **127**, 10575 (2016); https://doi.org/10.1016/j.ijleo.2016.08.063
7. J.K. Li, J.G. Li, S.H. Liu, X.D. Li, X.D. Sun and Y.S. Sakka, *J. Mater. Chem. C Mater. Opt. Electron. Devices*, **1**, 7614 (2013); https://doi.org/10.1039/c3tc31413h
8. C.S. Kamal, T.K. Visweswara Rao, P.V.S.S.S.N. Reddy, K. Sujatha, B.P. Ajayi, J.B. Jasinski and K.R. Rao, *RSC Adv.*, **7**, 9724 (2017); https://doi.org/10.1039/C6RA28719K
9. T. Samuel, C.S. Kamal, S. Ravipati, B.P. Ajayi, V. Veeraiah, V. Sudarsan and K.R. Rao, *Opt. Mater.*, **69**, 230 (2017); https://doi.org/10.1016/j.optmat.2017.04.037
10. N. Lakshminarasimhan and U. Varadaraju, *Mater. Res. Bull.*, **41**, 724 (2006); https://doi.org/10.1016/j.materresbull.2005.10.010

11. D. Lybye, F.W. Poulsen and M. Mogensen, *Solid State Ion.*, **128**, 91 (2000); https://doi.org/10.1016/S0167-2738(99)00337-9
12. C. Guo, X. Ding, L. Luan and Y. Xu, *Sens. Actuators B Chem.*, **143**, 712 (2010); https://doi.org/10.1016/j.snb.2009.10.023
13. M. Xie, D. Li, R. Pan, X. Zhou and G. Zhu, *RSC Adv.*, **5**, 22856 (2015); https://doi.org/10.1039/C5RA00585J
14. S. Park, *Mater. Lett.*, **135**, 59 (2014); https://doi.org/10.1016/j.matlet.2014.07.134
15. S. Lee and S. Park, *J. Lumin.*, **143**, 215 (2013); https://doi.org/10.1016/j.jlumin.2013.05.008
16. K. Li, H. Lian, M. Shang and J. Lin, *Dalton Trans.*, **44**, 20542 (2015); https://doi.org/10.1039/C5DT03565A
17. Z. Sun, M. Wang, Z. Yang, Z. Jiang, K. Liu and Z. Ye, *J. Alloys Compd.*, **658**, 453 (2016); https://doi.org/10.1016/j.jallcom.2015.10.242
18. C. Hu, Z. Zhang, H. Liu, P. Gao and Z.L. Wang, *Nanotechnology*, **17**, 5983 (2006); https://doi.org/10.1088/0957-4484/17/24/013
19. L. Chen, K.J. Chen, S.F. Hu and R.S. Liu, *J. Mater. Chem.*, **21**, 3677 (2011); https://doi.org/10.1039/c0jm02487b
20. J. Heyd, G.E. Scuseria and M. Ernzerhof, *J. Chem. Phys.*, **118**, 8207 (2003); https://doi.org/10.1063/1.2204597
21. S. Dudarev, G. Botton, S. Savrasov, C. Humphreys and A. Sutton, *Phys. Rev. B*, **57**, 1505 (1998); https://doi.org/10.1103/PhysRevB.57.1505
22. X. Hu, F. Piccinelli and M. Bettinelli, *J. Alloys Compd.*, **889**, 163344 (2022); https://doi.org/10.1016/j.jallcom.2021.163344
23. H. He, R. Fu, Y. Cao, X. Song, Z. Pan, X. Zhao, Q. Xiao and R. Li, *Opt. Mater.*, **32**, 632 (2010); https://doi.org/10.1016/j.optmat.2010.01.009
24. S. Dutta, S. Som and S.K. Sharma, *Dalton Trans.*, **42**, 9654 (2013); https://doi.org/10.1039/c3dt50780g